Published in final edited form as:
Nat Neurosci. ; 15(4): 628–635. doi:10.1038/nn.3064.

Decorrelation and efficient coding by retinal ganglion cells

Xaq Pitkow[1] and **Markus Meister**[2]

Markus Meister: meister@fas.harvard.edu

[1]Department of Brain and Cognitive Sciences, University of Rochester

[2]Molecular and Cellular Biology, Center for Brain Science, Harvard University, 52 Oxford St, Cambridge, MA 02138, 617-496-8301

Abstract

An influential theory of visual processing asserts that retinal center-surround receptive fields remove spatial correlations in the visual world, producing ganglion cell spike trains that are less redundant than the corresponding image pixels. For bright, high-contrast images, this decorrelation would enhance coding efficiency in optic nerve fibers of limited capacity. Here we test the central prediction of the theory and demonstrate that the spike trains of retinal ganglion cells are indeed decorrelated compared to the visual input. However, most of the decorrelation is accomplished not by the receptive fields, but by nonlinear processing in the retina. We show that a steep response threshold enhances efficient coding by noisy spike trains, and the effect of this nonlinearity is near optimal in both salamander and macaque retina. These results offer an explanation for the sparseness of retinal spike trains, and highlight the importance of treating the full nonlinear character of neural codes.

Introduction

The optic nerve limits how much visual information the eye can transmit to the brain. Early workers postulated that the early visual system is designed to use that limited information capacity efficiently, reducing the redundancy in natural scenes by discarding information that the brain has already received from another source in space or time[1,2]. Subsequently this idea was formalized mathematically[3–8], postulating that the retina transmits visual information to the brain optimally within limits imposed by optic nerve capacity. Images from the natural world have strong, uninformative correlations between the signals carried by different pixels[9]. An efficient encoder could suppress these by spatially filtering the image. Based on a model of the retina with several simplifying assumptions, one can compute the optimal spatial filter, and it resembles the familiar center-surround receptive fieldsof retinal ganglion cells [5,10]. By computing the difference between the intensity at a point and the average intensity at nearby points, this filter indeed removes spatial correlations in the retinal image, up to some limit determined by photoreceptor noise. This idealized retina model correctly predicts the spatial sensitivity of human vision[6] and several other psychophysical laws[8].

Despite the decorrelation theory's successful predictions, there has been no experimental test whether neural activity is in fact decorrelated at the putative bottleneck of the optic nerve. One study confirmed that neural firing in the cat's lateral geniculate nucleus is decorrelated in time [11], but there was no test of correlations across space. Another reported both spatial and temporal decorrelation by second-order fly visual neurons[7]. However, the

Author contributions

XP and MM designed the study; XP performed all experiments, analysis, and modeling; XP and MM wrote the article.

stimuli in this study were still images scanned over the retina, confounding the spatial and temporal contributions to visual processing. A third study found that retinal ganglion cells oversample visual space, resulting in substantial redundancy [12], but this oversampling may exist either with or without decorrelation relative to the stimulus. Thus one is still left with these basic questions: Does retinal processing indeed decorrelate signals at different spatial locations? If so, does this decorrelation improve coding efficiency?

We inspected spatial and temporal decorrelation in the retina, by recording from a population of retinal ganglion cells (RGCs) while presenting a stimulus with the spatio-temporal correlation structure of natural scenes[9]. We then compared the correlations among RGC spike trains to the correlations between corresponding image locations. To understand how the decorrelation occurs, we analyzed separately the contributions from center-surround receptive fields, noise, and sparsifying nonlinearities in the retinal network. We conclude that the dominant effect comes not from the receptive field, but from the nonlinear stimulus-response relationship. These nonlinearities exhibit high response thresholds that lead to sparse firing rates. We show that these attributes permit neurons to transmit information with nearly optimal efficiency.

Results

Our goal was to test whether retinal circuits remove the spatio-temporal correlations present in natural scenes, and if so, to explain whether this helps encode the stimulus efficiently. We therefore measured correlation as a function of distance and time lag in both the visual input and the RGC output. We recorded spike trains from many ganglion cells in the isolated salamander retina under two visual stimuli: One ("naturalistic") consisted of pseudo-random gaussian flicker with long-range spatio-temporal correlations like those of natural scenes (Figs. 1a, **S1**); the other ("white noise") was a flicker stimulus without correlations (Fig. 1b). The stimuli were bright, in the photopic regime, where the efficient coding theory predicts that decorrelation is the optimal strategy[4,7].

Retinal ganglion cells decorrelate the visual input

The typical ganglion cell responded to such displays with precisely timed bursts of spikes separated by complete silence (Fig. 1c). We measured each neuron's spatio-temporal receptive field (Figs. 1d–e) by the standard reverse-correlation method [13]. Then we computed the correlation function between the spike trains of any two neurons (Fig. 1f). These correlation functions generally showed a central peak of ~50 ms width; this was also the characteristic time scale for variations in the firing rate (Fig. 1c). Thus we focused our analysis on the correlations of spike counts in 50-ms time windows (see Methods).

Figure 1g–h plots the firing correlation for every pair of ganglion cells against the retinal distance between their receptive field centers. This can be compared to the spatial correlations in the stimulus. During white-noise stimulation, the correlation in the firing of ganglion cells greatly exceeded the stimulus correlation out to ~300μm (Fig. 1g). This is because the receptive field centers of nearby RGCs overlap (Fig. 1e), so they receive correlated input from their shared photoreceptors. By contrast, under the naturalistic stimulus, neural responses were dramatically less correlated than the stimulus pixels (Fig. 1h). The ganglion cells exhibited significant correlations only to ~400 μm distance, while the stimulus correlations extended at least twice as far. These observations held for distinct cell types [14,15] analyzed separately (data not shown). Thus the retina does decorrelate stimuli with natural image statistics, while introducing excess correlation under the unnatural white-noise ensemble. This much is in accordance with the classical efficient coding theory.

Decorrelation is achieved primarily by retinal nonlinearities

However, the theory also specifies a decorrelation mechanism, namely center-surround antagonistic receptive fields [2–4,7]. Owing to this antagonism, a retinal ganglion cell fires less to stimuli with low spatial frequency — which drive center and surround equally — and more to those with high spatial frequency[16]. But the low-frequency patterns are precisely those that synchronize nearby neurons. Consequently, a center-surround receptive field should reduce spatial correlations in the retinal output.

To test this, we measured how much decorrelation could be attributed to receptive field filtering: We convolved each spatio-temporal receptive field (Fig. 1d) with the naturalistic visual stimulus, and analyzed the remaining correlations (Fig. 2a–b). Filtering by the receptive field center alone extended the range of correlations, but addition of the antagonistic surround indeed reduced them below the correlations in the stimulus (Fig. 2a) as predicted by the theory, especially at distances beyond one center diameter, ~300 μm (Fig. 2a). However, unlike the theoretical prediction, this decorrelation was far from complete. Under the high-contrast stimuli used here, the optimal linear filters should reduce the correlations to nearly zero [4] for distances greater than the center diameter. Instead, the experimentally measured receptive fields left substantial correlations out to distances twice as great (Fig. 2a–b), falling far short of the theoretical prediction.

By comparison, the actual decorrelation achieved by the retina was very efficient: The measured correlations between ganglion cell spike trains were suppressed by a factor of ~3 even inside the receptive field center, and by more than ~10-fold outside (Fig. 2a–b). Clearly something other than receptive field filtering is responsible.

As illustrated in Figure 3, each ganglion cell fires in short stimulus-locked episodes, but with some trial-to-trial variation. The correlation between two such spike trains depends on the similarity of their firing events, and thus on (i) timing, (ii) sparseness, and (iii) trial-to-trial fluctuations or noise in each firing event (Fig. 3d).

The timing of a ganglion cell's firing events is largely determined by its spatio-temporal receptive field, as confirmed by comparing the peaks in the filtered stimulus to those in the firing rate (Fig. 3b–c). However, measured firing events were narrower than the positive excursions of the linear model (Fig. 3b–c), presumably resulting from the many documented nonlinearities in the retina's response, including synaptic rectification, depression, gain control, spiking threshold, and refractoriness [17–20]. This sparsification means that firing events overlap in time much less than expected from receptive field processing. Indeed, correlations of the trial-averaged firing rates (Fig. 3b) lay far below those of the stimulus and those predicted from receptive field filtering alone (Fig. 2a). The effect is especially striking for neurons of opposite response polarity, where the retinal nonlinearities effectively abolish the pairwise correlations (Fig. 2b). Finally, we determined that trial-to-trial fluctuations in different neurons were largely independentunder the present stimulus conditions (Fig. S2). This noise further decorrelates the ganglion cell output (Fig. 2a–b). Such noise-induced effects are detrimental to efficient coding, but downstream circuits in the brain cannot distinguish decorrelation by noise from that achieved by other means.

One can now compare how much the different aspects of retinal processing contribute to decorrelating the retinal output. For instance, at 300 μm distance the natural stimulus contained strong correlations, but retinal processing subsequently reduced them by a total of 92% (Fig. 2a). Of this, the receptive field surround contributed ~25%; the sparsifying nonlinearities contributed ~60%; and noise was responsible for ~15% (Fig. 2c). Thus nonlinear processing in retinal circuits is by far the largest contributor to decorrelation at the

retinal output, whereas the much-touted center-surround receptive field makes only a minor contribution.

These observations applied to temporal correlations as well. Filtering the stimulus through the receptive field produces a mild reduction in the autocorrelation at short time delays, but also introduces strong anticorrelations at long delays (Fig. 2d). This results from the biphasic time course of the receptive field (Fig. 1d), analogous to the spatial antagonism between center and surround. By comparison, both the trial-averaged firing rate and noisy spike trains showed almost complete decorrelation, down to delays <100 ms (Fig. 2d). Again, one concludes that the filtering by receptive fields reduces stimulus correlations only marginally, whereas the sparsifying nonlinearities account for the bulk of temporal decorrelation in the retina.

To assess the generality of these results, we asked whether they extend also to primate retinas, and probably therefore to our own visual processing. Published spike trains show that macaque RGCs similarly produce sparse bursts separated by silence [21,22], an indication of substantial nonlinear processing also in the macaque retina. By analyzing the shapes of ganglion cell receptive fields [23,24] we confirmed that the center-surround filter explains only part of the decorrelation at the retinal output (Fig. 2e–f). On the other hand, the sparsifying nonlinearities in the response [23] make a substantial contribution. Note again the strong decorrelation of opposite response types (Fig. 2e) and the suppression of negative temporal correlations at long delays (Fig. 2f).

Decorrelation, sparseness, and efficient coding in the LNP model

To build intuition for these effects and prepare for further analysis, we consider briefly a simple, tractable model of neural signaling that has enjoyed some popularity in the study of retina, visual cortex, and other sensory modalities [25]. In the so-called LNP model, the visual stimulus is first convolved with a linear receptive field (L), producing a time-varying input signal. That signal is passed through an instantaneous nonlinearity (N), typically of sigmoid shape, producing a time-dependent firing rate, from which the spike train is generated by a Poisson process (P). The LNP model offers perhaps the simplest instance in which one can analyze the contributions of receptive field, nonlinearity, and noise to visual coding.

Consider two such neurons that process a Gaussian-distributed stimulus with different receptive field filters (Fig. 4a). The outputs of the two filters will be jointly Gaussian variables with a statistical dependency fully characterized by the correlation coefficient. Passage through the subsequent nonlinearity always reduces the correlation of the two signals (Fig. 4c–d), regardless of the shape of the nonlinearity[26]. For a monotonic sigmoid nonlinearity, a higher threshold produces greater decorrelation (Fig. 4c–d). An increase in threshold also lowers the mean firing rate, accounting for earlier observations that correlations decrease when firing rates are low [27]. Note that a nonlinearity with a high threshold has qualitatively different effects from one with low threshold: Whereas it suppresses positive correlation coefficients to a certain extent, it almost completely eliminates negative correlations (Fig. 4c–d). This is because two signals of opposite sign cannot cross threshold at the same time. These effects are very robust under different shapes of the nonlinearity (Fig. 4c), and likely explain why the observed anti-correlations between On and Off cells are so strongly suppressed by retinal nonlinearities (Fig. 2b). Finally, the effect of output noise is simply to reduce the correlation coefficient by a further factor (Fig. 4e). In sum, the basic relationships we demonstrated for actual retinal spike trains can be understood in the context of a simple model of nonlinear stochastic processing.

The classical theory of retinal decorrelation attributed that phenomenon to filtering by center-surround receptive fields, and explained its purpose as serving the efficient

transmission of visual information through the optic nerve. Given that most of the observed decorrelation is instead furnished by the nonlinear response function of the retina, one wonders whether this version of decorrelation is equally beneficial for efficient coding. We will explore this first in the context of the LNP model, and then compare the resulting predictions against the measured spike trains.

In the LNP model, the nonlinearity decorrelates if it has a high threshold (Fig. 4d) ensuring that each neuron spends much of the time silent except for sharp and sparse firing events. This sparseness is prominent in the experimental responses (Fig. 1c) and has been observed across species[11,21,22,28,29]. This seems counterproductive for efficient information transmission. Why don't ganglion cells modulate their firing rate continuously to encode different stimulus values? Suppose a neuron must transmit an input signal that changes every time interval Δt by producing spikes during each interval according to a Poisson process with some firing rate. What mapping from input to firing rate maximizes the information rate in the spike train?

To explore this, we compared different monotonic sigmoid nonlinearities, as are often observed in fitting the LN model to visual neurons [23,30]. These can be described by three parameters: threshold, gain, and peak rate (Fig. 4b). We take the filtered stimulus to have a normal distribution; this is guaranteed by construction for our Gaussian naturalistic stimulus, and by the central limit theorem for the white noise stimulus because the receptive fields extend over many stimulus values in space and time. Now one can compute the mutual information between stimulus and spike train for any shape of the nonlinearity. Clearly the information can be increased arbitrarily by simply raising all the firing rates, so we fixed the mean firing rate to a value realistic for RGCs. That constraint leaves only two free shape parameters for the nonlinearity, for example the threshold and the gain.

As seen in Fig. 4f, at very high thresholds the information transmission is poor. In this regime the neuron reports only the rare threshold crossings, firing a burst of spikes each time to match the mean firing rate. Surprisingly, transmission also drops at low thresholds. In this condition, the neuron fires in many of the time bins, and thus the spike counts must be low, to satisfy the average rate constraint. But in a Poisson process, low spike counts are associated with high relative variability. Thus the choice of threshold involves a tradeoff between rarely using reliable symbols, namely high spike counts, or frequently using unreliable symbols, namely low spike counts. The optimum is found at an intermediate threshold value.

The optimal gain of the model neuron was infinite (Fig. 4f), with complete silence for stimuli below threshold and maximal firing rate for those above. This result runs counter to the conventional view of neural coding as a graded modulation of the firing rate, though related predictions have been in the theory literature for some time [31,32]. For the parameters that characterize a typical salamander ganglion cell from our experiments (coding window $\Delta t = 50$ ms, average firing rate = 1.1 Hz), one finds that the optimal neuron should remain silent 94.5% of the time and fire at 20 Hz the remaining 5.5% of the time. Thus efficient coding theory predicts that under the present constraints on firing rate and dynamics a neuron should indeed fire sparsely, with brief firing events separated by periods of silence.

Sparse firing enhances coding efficiency of ganglion cells

How close do empirically observed firing rates come to optimal performance? Here we make the approximation that the dominant source of noise in ganglion cell responses arises at the output, after all of the retina's nonlinear processing has taken place, for example during spike generation. In that case, the information transmission rate about the stimulus depends only on the probability distribution of the ganglion cell's firing rate, not how it is

generated (Eqn 18). Figure 5a illustrates the cumulative distribution of the firing rate for three sample ganglion cells. In most time bins the measured rate is exactly zero, followed by a long tail in the distribution out to high values. These distributions are fit well by a 3-parameter expression (Eqn 19). How efficient are these distributions of the firing rate for information transfer?

For comparison we identified the firing rate distribution with the same mean that uses spikes most efficiently. Because real ganglion cell spike trains do not conform exactly to Poisson statistics[17,21,33] we used an empirically fit noise model (Eqn 11, Fig. S2). The dependence of information rate on the shape of the firing rate distribution is shown in Fig. 5b. The optimum, as for the LNP model considered above, is a binary distribution that uses just two firing rates. But there is a corridor of high efficiency leading to that point, and almost all the measured rate distributions lay within that domain. Indeed when we computed the information transmission directly from the spike trains (Methods), the median RGC had a coding efficiency of 73% compared to the theoretical optimum (Fig. 5c).

Again, we found that these results extend to responses from primate retinal ganglion cells. While their mean firing rates are higher, the correlation time of the response and thus the effective bin width for spike train signaling is shorter, on the order of $\Delta t = 10$ ms [21]. We analyzed published distributions of the firing rate and the trial-to-trial noise [21] and computed information transmission rate as before. The sparse responses of macaque neurons allow a transmission rate close to the optimum, with a median efficiency of 81% (Fig. 5d).

In summary we have shown that a treatment of efficient coding theory that incorporates nonlinear transforms and noisy spike trains can explain the paradoxical nature of high-threshold nonlinearities and sparse responses in retinal processing.

Discussion

We have extended the application of efficient coding theory in the retina to considerably more realistic conditions. The classic approach treated the early visual system as a linear filter, with graded output signals, gaussian noise, and an average power constraint[4,7], none of which describes the real retina. We now allow for nonlinear processing, a spiking output with stochastic noise, and a constraint on the overall firing rate, as might be dictated by metabolic cost[34]. These extensions deliver new insights into the nature of retinal processing.

Two forms of redundancy reduction

The prominent decorrelation of signals in the retinal output is now seen as deriving primarily from two very different mechanisms (Figs. 2–4). The first is a linear spatio-temporal filter that implements lateral inhibition in space and biphasic responses in time. This conforms to the classic notion that the retina seeks to reduce redundancy between parallel channels in space and within a channel across time[2], though this reduction is incomplete (Fig. 2). The second, more substantial contribution derives from nonlinear processing in each individual channel (Figs. 2–3) which efficiently matches visual signals to the available coding symbols (Figs. 4–5). This second stage reduces the coding redundancy within each output channel resulting from inefficient symbol use. These observations apply for ganglion cells of multiple types in such different species as salamander and macaque (Figs. 2, 5), suggesting that our extension of the efficient coding framework has some general utility.

Validity of the assumptions

While the model of retinal processing used here is considerably more realistic than in the classical linear decorrelation theory, it is worth inspecting the remaining approximations.

For our first claim, that the receptive field filters contribute only a fraction of the decorrelation, we used a standard method to measure receptive fields, namely reverse correlation of the response to white noise stimuli [13]. Although receptive fields can adapt to the pattern of stimulation [35], we found that surrounds estimated under naturalistic stimulation narrowed only slightly and did not decorrelate any more than those obtained with white noise (data not shown).

Our second claim, that high-threshold nonlinearities enhance efficient coding, assumes that photoreceptor noise is negligible. This is the regime in which the classical theory predicts decorrelation of the retinal output. We also use this assumption in estimating the information rates in spike trains. The high light levels used in the experiments are designed to favor low photoreceptor noise. Any remaining input noise would be shared by ganglion cells with overlapping receptive fields, but we found noise correlations to be very small (Fig. S2). This suggests that indeed most of the noise in the RGC responses arises close to the output, rather than in shared presynaptic sources.

Our analysis of information transmission follows a classic approach [31], and requires choice of a coding window Δt, the time scale on which RGCs can completely change their firing rates to different values. We adopted $\Delta t = 50$ ms for salamander ganglion cells based on the observed width of firing events (Fig. 3a–b) and their autocorrelation function (Fig. 2f). We varied Δt in the analysis and found that the general conclusions are insensitive to small changes in this parameter: Sparse firing provides the most efficient code as long as the mean spike count remains considerably less than one spike per time bin.

Our models of signal and noise within the coding window do not specify a particular mechanism of spike generation. However, it is worth noting that the experimentally observed distributions of the firing rate (Fig. 5a) and the noise (Fig. S3) are readily produced by mechanistic models like a leaky integrate-and-fire neuron with gaussian subthreshold noise (data not shown).

Incomplete decorrelation by receptive fields

One outcome of this study was that the spatial receptive fields of ganglion cells fail to decorrelate retinal signals as completely as expected from the classical theory (Fig. 2a). Basically, the antagonistic surround of the receptive field is weaker than predicted. With high luminance and high contrast considered here, the theory predicts that the integrated strength of the surround should precisely cancel the center (Eqn 2.4 of ref 10). The receptive fields we observed have much weaker surrounds, and thus decorrelate less. This is also evident in preceding work: In macaque RGCs, the surround amounts to only ~50% of the center (Fig. 10 of ref 36). Note that while the original studies always wrote about “retinal filters” for spatial decorrelation, their tests of the theory used comparisons to human psychophysics, and thus included post-retina stages of decorrelation (Figs. 1 and 4 of ref 4).

A plausible explanation why the linear receptive fields fail to decorrelate much is that they don’t entirely reflect what these retinal ganglion cells compute. Many of these neurons are selective for quite specific visual features, like motion in a particular direction [37], differential motion [38], or local edges [39]. This selectivity arises from diverse nonlinearities [40] and is poorly represented in the spatio-temporal receptive field. Thus even neurons with strongly overlapping receptive fields may nonetheless never fire together. This recalls another feature of retinal organization that (so far) cannot be explained by efficient coding principles: the profusion of different ganglion cell types that each appear to compute a different visual message[41].

Nonlinearity and sparseness

Regardless of what a retinal ganglion cell computes, it must communicate the result downstream via noisy spike trains. To optimize information transmission using such a spiking process with a low mean activity, we found that retinal ganglion cells should be silent most of the time, and fire at a high rate only rarely. This expectation holds over all the experimental conditions we analyzed, for all the salamander ganglion cells, and all but one of the macaque neurons. The actual measured nonlinearities were not quite infinitely sharp, but matched the expected threshold closely (Fig. 5).

Interestingly, the theory behind this was developed already some time ago. Stein[31] discovered by numerical methods that a Poisson process transmits maximal information using a discrete set of firing rates — only two if the maximal rate is strongly limited. The result was later proved analytically in studies of fiber-optic communication [32]. Nevertheless these facts are poorly appreciated among neuroscientists, even though Poisson models are used ubiquitously. Most of us (authors included) assumed neurons should modulate their firing rate continuously to benefit from all possible rates. This intuition was formalized in an influential paper [42] that derived a smooth sigmoid as the optimal shape of the response function. But that treatment was for a continuous output signal, like membrane potential, and a constant additive noise level. The fact that the spike train is a point process with output-dependent noise ultimately leads to the counter-intuitive step-shaped nonlinearity. This behavior has been derived under a constraint on the maximal firing rate [32]. We showed here that discrete firing rate distributions arise also when the constraint applies instead to the mean rate (Fig. 4f).

The sparse responses of RGCs under naturalistic stimulation can now be seen as maximizing coding efficiency in single spike trains within the optic nerve bottleneck. In the cortex, sparse coding has been interpreted differently, as a useful strategy for learning and processing spike patterns[43] or to extract large signals from background noise [44]. These arguments are plausible for highly overcomplete representations, where — unlike in the retina — the number of neurons greatly exceeds the stimulus dimensionality. Still, one might imagine that even in the cortex, the driving force for sparseness is really communicating efficiently with Poisson spike trains[45].

Decorrelation and efficient coding

Correlation is often considered a proxy for information-theoretic redundancy, with the implication that decorrelation somehow improves efficiency. Certainly high correlation does imply strong statistical dependence, but weak correlation need not imply weak dependence: Correlation is a second-order measure, and fully reflects the redundancy between two signals only if they are normally distributed. For highly non-gaussian signals like neural spike trains and natural images, correlation may be only weakly related to redundancy. For example, the nonlinearity of the LNP model dramatically decreases the correlation between neural responses (Fig. 4d) while actually increasing their statistical dependency (Fig. 4g). Correlation and efficiency also have a complex relationship. For instance, if two signals are affected by independent noise, this decorrelates them without improving coding efficiency. Nonlinearities invariably decorrelate two gaussian signals, but may not improve coding efficiency. Nonetheless, many studies of neural signaling simply measure correlation and leave the impression that decorrelation alone is evidence of improved efficiency[46–50]. These examples illustrate that all decorrelations are not created equal. Though many neural circuits perform some decorrelation of their inputs, one must distinguish the various forms of this phenomenon, because they are implemented by very different mechanisms and play different roles for the neural code.

Methods

Recording

Experiments were performed on the isolated retina of the larval tiger salamander, superfused with oxygenated Ringer's solution, following protocols approved by the IACUC at Harvard University. Action potentials from retinal ganglion cells were recorded extracellularly with a multi-electrode array[51]. Neurons were selected for analysis if they maintained steady firing rates throughout the two-hour experiments and their spike waveforms could be sorted unambiguously. 103 cells from nine retinas satisfied this criterion. Classification into different cell types was achieved by agglomerative maximum-linkage clustering according to the Euclidean distances between temporal receptive fields[14,15]. Of the recorded cells, 6 were classified as ON cells, 18 as slow OFF cells, and 79 as fast OFF cells. Altogether this yielded 5356 response pairs, including comparisons across experiments.

Stimulation

Light was projected from a computer monitor onto the photoreceptor layer. The stimulus was a square grid with fields of size (54 μm) ^{2} covering a total area of (3.4 mm)^2. The monitor refresh interval was 15 ms. The mean light level at the retina (7×10^{-3} W/m^2) was in the regime of photopic vision[51].

The decorrelation theories assumed that light intensities in visual stimuli are drawn from a correlated multivariate normal distribution exhibiting the spatial power spectrum measured for natural scenes[9], which varies with spatial frequency $\mathbf{k}$ as $1/|\mathbf{k}|^2$. These assumptions neglect objects, edges, and textures but capture pairwise intensity correlations in the visual world. To address these theories directly we designed spatiotemporal stimuli that approximated the pairwise correlations in natural stimuli and neglected all higher-order structure.

We generated the spatial structure of the stimulus $S(\mathbf{x}, t)$ by drawing spatial frequency coefficients $\tilde{S}_0(\mathbf{k}, t)$ independently every 15 ms from a gaussian distribution with variance proportional to $1/|\mathbf{k}|^2$. Temporal correlations were introduced by low-pass filtering the spatial frequency coefficients with an exponential of time constant $\tau = 1/|\mathbf{k}|\nu$, where ν is a constant with units of velocity that determines the scaling between space and time. This constant was set to ν=10°/sec, corresponding to a typical velocity that elicits neural and behavioral responses in salamanders in visual tasks[52]. The spatial frequency coefficients were given by

$$\tilde{S}(\mathbf{k}, t) = Ae^{-t/\tau} \circ \tilde{S}_0(\mathbf{k}, t) \quad (1)$$

where ◦ represents a temporal convolution and the constant A fixed the overall contrast (the ratio of standard deviation of luminance to mean luminance) at 35%. An inverse spatial Fourier transform generated each image frame for display (Fig. 1a). The overall spatiotemporal power spectrum at spatial frequency $\mathbf{k}$ and temporal frequency ω is

$$\tilde{P}(\mathbf{k}, \omega) \propto \frac{1}{|\mathbf{k}|^2} \cdot \frac{1-e^{-2|\mathbf{k}|\nu\Delta t}}{1+e^{-2|\mathbf{k}|\nu\Delta t}-2e^{-|\mathbf{k}|\nu\Delta t}\cos\omega\Delta t} \quad (2)$$

(Fig. S1). This spectrum closely approximates that of natural movies [53]: In the limit of low spatial frequency it becomes $|\mathbf{k}|^{-3} f(\omega/|\mathbf{k}|)$ for a function f peaked at zero in the ratio $\omega/|\mathbf{k}|$. In this limit the power varies with temporal frequency approximately as ω^{-2}, as observed[53].

The stimulus has qualitative similarities with natural scenes: Large features are more prominent, and persist longer, than small details.

To compare the results from macaque and salamander, we used the same stimuli, except that the stimulus checker size was scaled in proportion to the mean ganglion cell receptive field radius.

Correlation

The correlation between two signals x and y was quantified by the second-order correlation function,

$$C_{xy}(\tau)=\frac{\langle \Delta x(t)\cdot \Delta y(t+\tau)\rangle}{\sqrt{\langle \Delta x^2(t)\rangle \langle \Delta y^2(t)\rangle}} \quad (3)$$

where Δx and Δy represent deviations of x and y from their respective means and $\langle\cdot\rangle$ symbolizes an average over time. To reduce high-frequency noise, each signal was first binned into windows of width Δt =50 ms for salamander neurons and 10 ms for primate neurons. This sets the time resolution on which the neural responses are analyzed. These values were chosen because they reflect the time scale on which ganglion cell firing varies: the typical duration of a stimulus-evoked burst of spikes [28] (Fig. 1c) and the width of the peak in the temporal receptive field (Fig. 1d).

Because the shared noise sources were small (Fig. S2) we focused on stimulus-driven correlations, by presenting the same stimulus twice and computing correlations between the spike trains across the two repeats.

The correlation measure (Eqn 3) was computed the same way for pairs of stimulus values, trial-averaged firing rates, spike trains, or the outputs of various functional models. In graphs of correlation versus spatial distance, we plotted the correlation at zero delay, C_{xy} (0). For visualization we binned the cell pairs by distance into groups of 100 and plotted the median for each group (Fig. 1g–h, Fig. 2). Distances were quantified as the separation between the midpoint of the receptive fields.

Receptive Fields

To map the receptive fields we applied a random checkerboard stimulus[51] with a temporal sampling rate of 22 Hz and (54 μm)^2 black or white checkers. To reduce noise in the receptive field estimate, we fitted each neuron's spatiotemporal receptive field with a direct product of a spatial receptive field and a temporal kernel,

$$F(\mathbf{x},t)\approx X(\mathbf{x})T(t) \quad (4)$$

using singular value decomposition. Each neuron's position was assigned as the midpoint of a 2D gaussian fit to its spatial receptive field $X(\mathbf{x})$ (Fig. 1e).

For modeling primate receptive fields we parametrized $X(\mathbf{x})$ and $T(t)$ as

$$X(\mathbf{x})=\frac{1}{2\pi\sigma_c^2}e^{-|\mathbf{x}-\mu_c|^2/2\sigma_c^2}-a\frac{1}{2\pi\sigma_s^2}e^{-|\mathbf{x}-\mu_s|^2/2\sigma_s^2} \quad (5)$$

$$T(t)=(t/\tau_1)^{n_1}\, e^{-n_1(t/\tau_1-1)}-b(t/\tau_2)^{n_2}\, e^{-n_2(t/\tau_2-1)} \quad (6)$$

with spatial parameters drawn from Croner and Kaplan[36] for the parafovea (5°–10° eccentricity) and temporal parameters drawn from Chichilnisky and Kalmar[23].

Given a receptive field $F(\mathbf{x}, t)$ we computed the linear prediction $r(t)$ for the neural response by convolution with the stimulus:

$$r(t)=\iiint d^2\mathbf{x}\,d\tau F(\mathbf{x},\tau)S(\mathbf{x},t-\tau) \quad (7)$$

Nonlinearities

In the Linear-Nonlinear (LNP) model, the linear prediction $r(t)$ is transformed into a firing rate $\rho(t)$ by an instantaneous nonlinearity $N(\cdot)$,

$$\rho(t)=N(r(t)) \quad (8)$$

and then into a spike count, n, by drawing from a Poisson distribution with that rate

$$P(n|\rho)=\frac{e^{-\rho\Delta t}(\rho\Delta t)^n}{n!} \quad (9)$$

where Δt is the time bin. We parametrized the nonlinearity as a sigmoid using the logistic function

$$N(r)=K/\left(1+e^{-g(r-\theta)}\right) \quad (10)$$

with peak firing rate K, gain g, and threshold θ.

If the linear input $r(t)$ follows a normal distribution, one can constrain the mean firing rate of the model neuron to a value μ, by setting the peak rate to

$K=\mu\sqrt{2\pi}/\int dr\, e^{-\frac{1}{2}r^2}\left(1+e^{-g(r-\theta)}\right)^{-1}$.

Noise

Large bursts of spikes from ganglion cells are more regular than expected from Poisson statistics[17,21,28], so the Poisson model generally overestimates the noise. For some computations (Fig. 5b–d) we used a noise distribution measured empirically. For a given mean spike count ρ at a given time during the trial, the measured spike count distributions $P(n\rho)$ had a width that stayed constant with ρ after an initial Poisson-like growth (Fig. S3). These distributions were well-described as a gaussian distribution on non-negative integer spike counts,

$$P(n|\rho)\propto\exp\left[-\frac{(n-n_0(\rho))^2}{2\sigma^2}\right]\quad n=0,1,2,\ldots \quad (11)$$

where $n_0(\rho) = a\log(1 + e^{\rho\,\Delta t/a})$ is the center of the gaussian and σ is the width of the noise distribution. For each σ, the parameter a was set so the conditional mean of the model noise

distribution closely approximated the desired mean ρ. The noise width σ was fit by numerically maximizing the log-likelihood, $\Sigma_{t,i} \log P(n(t,i) \rho(t);\sigma)$, where $n(t, i)$ is the measured spike count in bin t during stimulus repetition i.

Our models assume that noise affects the spiking of each neuron independently, whereas nearby ganglion cells share certain noise sources, especially at low light levels[54,55]. We found at photopic intensities that noise correlations were very small, <0.01 for 90% of pairwise comparisons (Fig. S2). This justified the independent noise approximation for the great majority of cells, which simplifies the treatment of optimal coding. Another study has reported that response models which account for noise correlations in ganglion cell spike trains can extract additional (~20%) visual information[22].

Decorrelation by nonlinearities and noise

The correlation between two LNP model neurons depends on both the nonlinearities and the noise (Fig. 4). Suppose that the inputs x and y to two neurons are both normally distributed with zero mean and unit variance and correlation coefficient c. After transformation by the nonlinear function $N(\cdot)$, the correlation coefficient becomes

$$C_{N(x)N(y)} = \frac{\langle N(x)N(y)\rangle - \mu^2}{\sigma^2} \quad (12)$$

where the nonlinear output has mean $\mu = \langle N(x)\rangle$ and variance $\sigma^2 \langle = N^2(x)\rangle - \mu^2$, and where $\langle\ \rangle$ is an expectation over the input distribution,

$$P(x,y) = \frac{1}{2\pi\sqrt{1-c^2}} \exp\left(-\frac{1}{2}\frac{x^2 - 2xyc + y^2}{1-c^2}\right) \quad (13)$$

We computed these expectation values by numerical integration (Figs. 4b–d).

Response noise increases the variance without altering the covariance, lowering the correlation. For two conditionally independent signals x and y with (time-dependent) trial averages of $\bar{x}$ and $\bar{y}$, the noise is $\delta x = x - \bar{x}$ and $\delta y = y - \bar{y}$. The correlation between the noisy signals x and y is then

$$C_{xy} = \frac{\langle \overline{xy}\rangle - \langle \bar{x}\rangle \langle \bar{y}\rangle}{\sqrt{\langle \bar{x}^2\rangle - \langle \bar{x}\rangle^2 + \langle \delta x^2\rangle}\sqrt{\langle \bar{y}^2\rangle - \langle \bar{y}\rangle^2 + \langle \delta y^2\rangle}} = C_{\bar{x}\bar{y}} \frac{1}{\sqrt{(1+1/SNR_x)(1+1/SNR_y)}} \quad (14)$$

where $C_{\bar{x}\bar{y}}$ is the correlation of the trial-averaged responses and $SNR_x = (\langle \bar{x}^2\rangle - \langle \bar{x}^2\rangle)/\langle \delta x^2\rangle$ is the ratio of signal variance to noise variance (Fig. 4e).

Information and efficiency for a single neuron

To analyze the role of nonlinearity in efficient coding, we computed the mutual information between the stimulus and the ganglion cell spike count in single windows of width Δt. This approximation neglects correlations between spike counts in different bins and spike timing within a bin. The mutual information between stimulus s and the spike count n is

$$I(n;s) = H(n) - H(n|s) \quad (15)$$

where the unconditional entropy $H(n)$ is

$$H(n)=-\sum_{n=0}^{\infty}p(n)\log p(n) \quad (16)$$

and the conditional entropy $H(n\,s)$ is

$$H(n|s)=-\int ds\, p(s)\sum_{n=0}^{\infty}p(n|s)\log p(n|s) \quad (17)$$

We calculated the mutual information in two ways: directly from neural responses, and using a response model. For the former, the integrals over all possible stimuli were replaced by temporal averages over the stimulus presentation. For the latter, the integrals over the high-dimensional stimulus ensemble are intractable. However, the model responses depend on the stimulus only through the time-varying firing rate $\rho(t)$. Assuming again that input noise is negligible, this firing rate is a deterministic function of the stimulus. Therefore, the conditional entropy given the stimulus equals the conditional entropy given the firing rate, $H(n\,s) = H(n\,\rho)$, and the mutual information is fully specified by the distribution of firing rates $p(\rho)$, regardless of how those rates arise:

$$I(n;s)=H(n)-H(n|s)=H(n)-H(n|\rho)=I(n;\rho) \quad (18)$$

Thus we compute entropies (Eqns 16–17) using $p(n) = \int d\rho\, p(n|\rho)p(\rho)$ and $p(n\,\rho)$ instead of $p(n) = \int ds\, p(n|s)p(s)$ and $p(n|s)$.

For the LNP model, the firing rate distribution is produced by the sigmoid nonlinearity $N(r)$ (Eqn 10) acting on the gaussian distributed linear input r. These distributions are parametrized like the logistic function, by the peak rate K, gain g, and threshold θ:

$$p(\rho)=\frac{K\exp\left[-\frac{1}{2}\left(\frac{1}{g}\log(K/\rho-1)-\theta\right)^2\right]}{\sqrt{2\pi}g\rho^2(K/\rho-1)} \quad (19)$$

This family of distributions encompasses a wide range of unimodal and bimodal shapes, including binary rate distributions when $g = \infty$.

To fit each ganglion cell response distribution (Fig. 5b, d) we minimized the mean squared difference between the cumulative distribution of the parametric model (Eqn 19)

$$D(\rho)-\frac{1}{2}\operatorname{erfc}\left(\frac{\log(K/\rho-1)-g\theta}{\sqrt{2}g}\right) \quad (20)$$

and the cumulative distribution of the measured firing rates. The median parameters over the recorded salamander cells were K=48 Hz, g=5.8, and θ=2.0. For primate neurons, fits were derived from published spike rasters [21], with median parameters K=72 Hz, g=2.8, and θ =0.95.

We numerically calculated the mutual information for the response model (Figs. 4f, 5b, 5d) by substituting the rate distribution (Eqn 19) and noise model (Eqn 11) into Eqns 15–17.

Given a neuron's mean firing rate μ, we determined the firing rate distribution that optimizes information transmission by numerically maximizing mutual information (Eqn 18) over the parameters g and θ in Eqn 19, setting

$$K=\mu\sqrt{2\pi}/\int dr\, e^{-\frac{1}{2}r^2}\left(1+e^{-g(r-\theta)}\right)^{-1} \quad (21)$$

to preserve the mean firing rate. Finally, we computed coding efficiency (Fig. 5c) by dividing the mutual information for the measured neural responses by this maximal information.

Information and redundancy for multiple correlated neurons

To compute the mutual information for a population of N LNP model neurons (Fig. 4g–h), we allowed the spike counts and firing rates in Eqns 15–17 to be N-dimensional vectors. We made several simplifications for tractability. First, all models had identicalthresholds θ, gains g, and peak firing rates K. Next, we assumed the input to the nonlinearities was a multivariate gaussian with uniform correlation matrix $\mathbf{\Sigma} = c + (1- c)\mathbf{I}$. Finally, we restricted the nonlinearity to have optimal (infinite) gain: Each neuron was either silent or fired at a maximal rate K in each time bin.

Given these simplifying assumptions, we can calculate the mutual information for the population. The unconditional probabilities of the vector of binary firing rates are

$$p(\boldsymbol{\rho})=\int_{O(\boldsymbol{\rho})} d^N\mathbf{r}\frac{1}{(2\pi)^{N/2}|\sum|^{1/2}}\exp\left(-\frac{1}{2}(\mathbf{r}-\theta)^T\sum^{-1}(\mathbf{r}-\theta)\right) \quad (22)$$

with integration over orthants $O(\boldsymbol{\rho})=\cap_i\{\mathrm{sgn}(\rho_i-\frac{K}{2})r_i>0\}$. We computed these integrals numerically, exploiting the model's permutation symmetry to reduce the number of integrals.

The model neurons are silent and have zero noise entropy if ρi=0, and emit spikes with probability

$$p(n_i|\rho_i=K)=\begin{cases} q & n_i=0 \\ 1-q & n_i>0 \end{cases} \quad (23)$$

and noise entropy

$$h(q)=-q\log q-(1-q)\log(1-q) \quad (24)$$

otherwise, with q=exp($-K\Delta t$) for Poisson noise. The conditional entropy (Eqn 17) is the average noise entropy across all firing rate patterns,

$$H(\mathbf{n}|\boldsymbol{\rho})=\sum_{\boldsymbol{\rho}}p(\boldsymbol{\rho})h(q)\sum_i\frac{\rho_i}{K} \quad (25)$$

The unconditional entropy (Eqn 16) is computed from the marginal spike count probability over spikes and silences, $p(\mathbf{n}) = \mathbf{\Sigma}_{\rho} p(\rho)\ \mathbf{\pi}_i\, p(n_i|\rho_i)$.

Redundancy (Fig. 4g) measures the difference between the total information conveyed by each neuron considered independently and the information all neurons convey together, compared to the information that could be conveyed if all neurons were independent, $R = \Sigma_i I(\rho_i; s) - I(\boldsymbol{\rho}; s) / \Sigma_i I(\rho_i; s)$.

Supplementary Material

Refer to Web version on PubMed Central for supplementary material.

Acknowledgments

We thank the members of the Meister laboratory, Mike Berry, Taro Toyozumi, Jean-Pierre Nadal, and an anonymous referee for helpful advice.

References

1. Attneave F. Some informational aspects of visual perception. Psychol Rev. 1954; 61:183–193. [PubMed: 13167245]
2. Barlow, HB. Possible principles underlying the transformation of sensory messages. In: Rosenblith, WA., editor. Sensory Communication. MIT Press; Cambridge, MA: 1961. p. 217-234.
3. Srinivasan MV, Laughlin SB, Dubs A. Predictive coding: a fresh view of inhibition in the retina. Proc R Soc Lond B Biol Sci. 1982; 216:427–459. [PubMed: 6129637]
4. Atick JJ, Redlich AN. What does the retina know about natural scenes? Neural Comput. 1992; 4:196–210.
5. Atick JJ, Redlich AN. Convergent algorithm for sensory receptive field development. Neural Comput. 1993; 5:45–60.
6. Atick JJ, Redlich AN. Could information theory provide an ecological theory of sensory processing? Network. 1992; 3:213–251.
7. van Hateren JH. Real and optimal neural images in early vision. Nature. 1992; 360:68–70. [PubMed: 1436076]
8. van Hateren JH. Spatiotemporal contrast sensitivity of early vision. Vision Res. 1993; 33:257–267. [PubMed: 8447098]
9. Field DJ. Relations between the statistics of natural images and the response properties of cortical cells. J Opt Soc Am A. 1987; 4:2379–2394. [PubMed: 3430225]
10. Atick JJ, Redlich AN. Toward a Theory of Early Visual Processing. Neural Comput. 1990; 2:308–320.
11. Dan Y, Atick JJ, Reid RC. Efficient coding of natural scenes in the lateral geniculate nucleus: Experimental test of a computational theory. J Neurosci. 1996; 16:3351–3362. [PubMed: 8627371]
12. Puchalla JL, Schneidman E, Harris RA, Berry MJ. Redundancy in the population code of the retina. Neuron. 2005; 46:493–504. [PubMed: 15882648]
13. Chichilnisky EJ. A simple white noise analysis of neuronal light responses. Network. 2001; 12:199–213. [PubMed: 11405422]
14. Warland DK, Reinagel P, Meister M. Decoding visual information from a population of retinal ganglion cells. J Neurophysiol. 1997; 78:2336–2350. [PubMed: 9356386]
15. Segev R, Puchalla J, Berry MJ. Functional organization of ganglion cells in the salamander retina. J Neurophysiol. 2006; 95:2277–2292. [PubMed: 16306176]
16. Enroth–Cugell C, Robson JG. Functional characteristics and diversity of cat retinal ganglion cells. Basic characteristics and quantitative description. Invest Ophthalmol Vis Sci. 1984; 25:250–267. [PubMed: 6698746]
17. Berry MJ, Meister M. Refractoriness and neural precision. J Neurosci. 1998; 18:2200–2211. [PubMed: 9482804]
18. Burrone J, Lagnado L. Synaptic depression and the kinetics of exocytosis in retinal bipolar cells. J Neurosci. 2000; 20:568–578. [PubMed: 10632586]

19. Demb JB, Zaghloul K, Haarsma L, Sterling P. Bipolar cells contribute to nonlinear spatial summation in the brisk–transient (Y) ganglion cell in mammalian retina. J Neurosci. 2001; 21:7447–7454. [PubMed: 11567034]
20. Field GD, Rieke F. Nonlinear signal transfer from mouse rods to bipolar cells and implications for visual sensitivity. Neuron. 2002; 34:773–785. [PubMed: 12062023]
21. Uzzell VJ, Chichilnisky EJ. Precision of spike trains in primate retinal ganglion cells. J Neurophysiol. 2004; 92:780–789. [PubMed: 15277596]
22. Pillow JW, et al. Spatio–temporal correlations and visual signalling in a complete neuronal population. Nature. 2008; 454:995–999. [PubMed: 18650810]
23. Chichilnisky EJ, Kalmar RS. Functional asymmetries in ON and OFF ganglion cells of primate retina. J Neurosci. 2002; 22:2737–2747. [PubMed: 11923439]
24. Croner LJ, Purpura K, Kaplan E. Response variability in retinal ganglion cells of primates. Proc Natl Acad Sci U S A. 1993; 90:8128–8130. [PubMed: 8367474]
25. Schwartz O, Pillow JW, Rust NC, Simoncelli EP. Spike–triggered neural characterization. J Vis. 2006; 6:484–507. [PubMed: 16889482]
26. Lancaster HO. Some properties of the bivariate normal distribution considered in the form of a contingency table. Biometrika. 1957; 44:289–292.
27. de la Rocha J, Doiron B, Shea–Brown E, Josic K, Reyes A. Correlation between neural spike trains increases with firing rate. Nature. 2007; 448:802–806. [PubMed: 17700699]
28. Berry MJ, Warland DK, Meister M. The structure and precision of retinal spike trains. Proc Natl Acad Sci U S A. 1997; 94:5411–5416. [PubMed: 9144251]
29. Reinagel P. How do visual neurons respond in the real world? Curr Opin Neurobiol. 2001; 11:437–442. [PubMed: 11502389]
30. Baccus SA, Meister M. Fast and slow contrast adaptation in retinal circuitry. Neuron. 2002; 36:909–919. [PubMed: 12467594]
31. Stein RB. The information capacity of nerve cells using a frequency code. Biophys J. 1967; 7:797–826. [PubMed: 19210999]
32. Shamai S. Capacity of a pulse amplitude modulated direct detection photon channel. IEE Proceedings–I Communications Speech and Vision. 1990; 137:424–430.
33. Keat J, Reinagel P, Reid RC, Meister M. Predicting every spike: a model for the responses of visual neurons. Neuron. 2001; 30:803–817. [PubMed: 11430813]
34. Balasubramanian V, Berry MJ. A test of metabolically efficient coding in the retina. Network. 2002; 13:531–552. [PubMed: 12463343]
35. Hosoya T, Baccus SA, Meister M. Dynamic predictive coding by the retina. Nature. 2005; 436:71–77. [PubMed: 16001064]
36. Croner L, Kaplan E. Receptive fields of P and M ganglion cells across the primate retina. Vision Res. 1995; 35:7–24. [PubMed: 7839612]
37. Barlow HB, Levick WR. The mechanism of directionally selective units in rabbit's retina. J Physiol. 1965; 178:477–504. [PubMed: 5827909]
38. Ölveczky BP, Baccus SA, Meister M. Segregation of object and background motion in the retina. Nature. 2003; 423:401–408. [PubMed: 12754524]
39. Levick WR. Receptive fields and trigger features of ganglion cells in the visual streak of the rabbits retina. J Physiol. 1967; 188:285–307. [PubMed: 6032202]
40. Gollisch T, Meister M. Eye smarter than scientists believed: Neural computations in circuits of the retina. Neuron. 2010; 65:150–164. [PubMed: 20152123]
41. Dacey, DM. Origins of perception: retinal ganglion cell diversity and the creation of parallel visual pathways. In: Gazzaniga, MS., editor. The Cognitive Neurosciences. MIT Press; Cambridge, MA: 2004. p. 281-301.
42. Laughlin SB. A simple coding procedure enhances a neuron's information capacity. Z Naturforsch. 1981; 36c:910–912.
43. Olshausen BA, Field DJ. Sparse coding of sensory inputs. Curr Opin Neurobiol. 2004; 14:481–487. [PubMed: 15321069]

44. Ringach DL, Malone BJ. The operating point of the cortex: neurons as large deviation detectors. J Neurosci. 2007; 27:7673–7683. [PubMed: 17634362]
45. van Vreeswijk CA. Whence sparseness? Advances in Neural Information Processing Systems. 2001; 13:189–195.
46. Vinje WE, Gallant JL. Sparse coding and decorrelation in primary visual cortex during natural vision. Science. 2000; 287:1273–1276. [PubMed: 10678835]
47. Wang XJ, Liu Y, Sanchez–Vives MV, McCormick DA. Adaptation and temporal decorrelation by single neurons in the primary visual cortex. J Neurophysiol. 2003; 89:3279–3293. [PubMed: 12649312]
48. Rucci M, Casile A. Fixational instability and natural image statistics: implications for early visual representations. Network. 2005; 16:121–138. [PubMed: 16411492]
49. Cleland TA. Early transformations in odor representation. Trends Neurosci. 2010; 33:130–139. [PubMed: 20060600]
50. Wiechert MT, Judkewitz B, Riecke H, Friedrich RW. Mechanisms of pattern decorrelation by recurrent neuronal circuits. Nat Neurosci. 2010; 13:1003–1010. [PubMed: 20581841]
51. Meister M, Pine J, Baylor DA. Multi–neuronal signals from the retina: acquisition and analysis. J Neurosci Methods. 1994; 51:95–106. [PubMed: 8189755]
52. Himstedt, W. Prey selection in salamanders. In: Ingale, DJ.; Goodale, MA.; Mansfield, RJW., editors. Analysis of Visual Behavior. MIT Press; Cambridge, MA: 1982. p. 47-66.
53. Dong DW, Atick JJ. Statistics of natural time–varying images. Network. 1995; 6:345–358.
54. Brivanlou IH, Warland DK, Meister M. Mechanisms of concerted firing among retinal ganglion cells. Neuron. 1998; 20:527–539. [PubMed: 9539126]
55. Schneidman E, Bialek W, Berry MJ. Synergy, redundancy, and independence in population codes. J Neurosci. 2003; 23:11539–11553. [PubMed: 14684857]

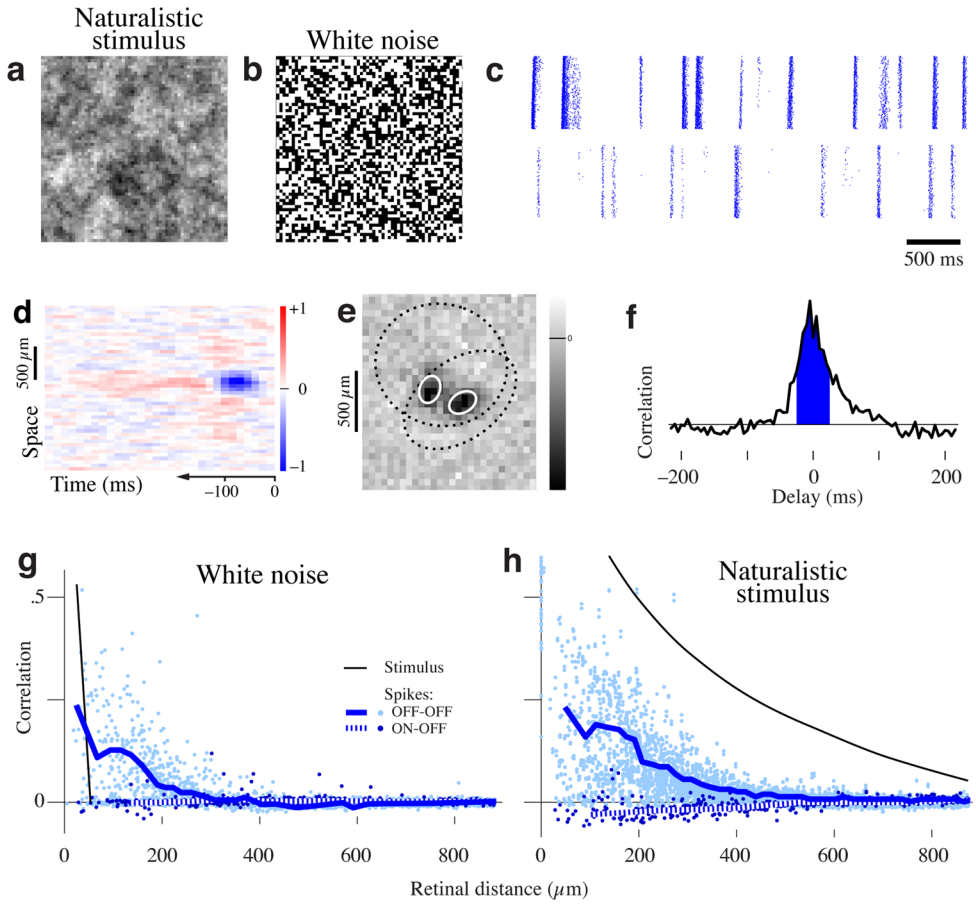

Figure 1.

Decorrelation of naturalistic stimuli. **a, b:** Sample frames of naturalistic and white noise stimuli, projected onto a 3.4mm square on the retina. **c:** Responses of two retinal ganglion cells to a short segment of the naturalistic stimulus, displayed as rasters of spikes on 250 identical repeats. **d:** A sample spatio-temporal receptive field for an OFF ganglion cell, measured as the spike-triggered average stimulus and integrated over one spatial dimension for ease of display. Note the spatial center-surround antagonism (red regions above and below blue) and the biphasic timecourse (red region left of blue). **e:** Spatial receptive fields of two OFF cells, including 1-s.d. outlines of the receptive field centers (solid) and surrounds (dotted). **f:** Cross-correlation function between two ganglion cell spike trains, indicating the frequency of spike pairs as a function of their delay. The shaded area encompasses most of the central peak and indicates the range of delays used to compute the quoted correlation coefficients. **g, h:** Correlation coefficient between the responses of two ganglion cells as a function of their distance under a white noise (g) or naturalistic (h) stimulus. Each pair of cells contributes a point; lines represent median correlation for pairs at similar distance. Comparisons are restricted within a cell type (solid lines) or across cell types (dashed lines). For reference, the correlation between stimulus pixels is shown as well (thin lines).

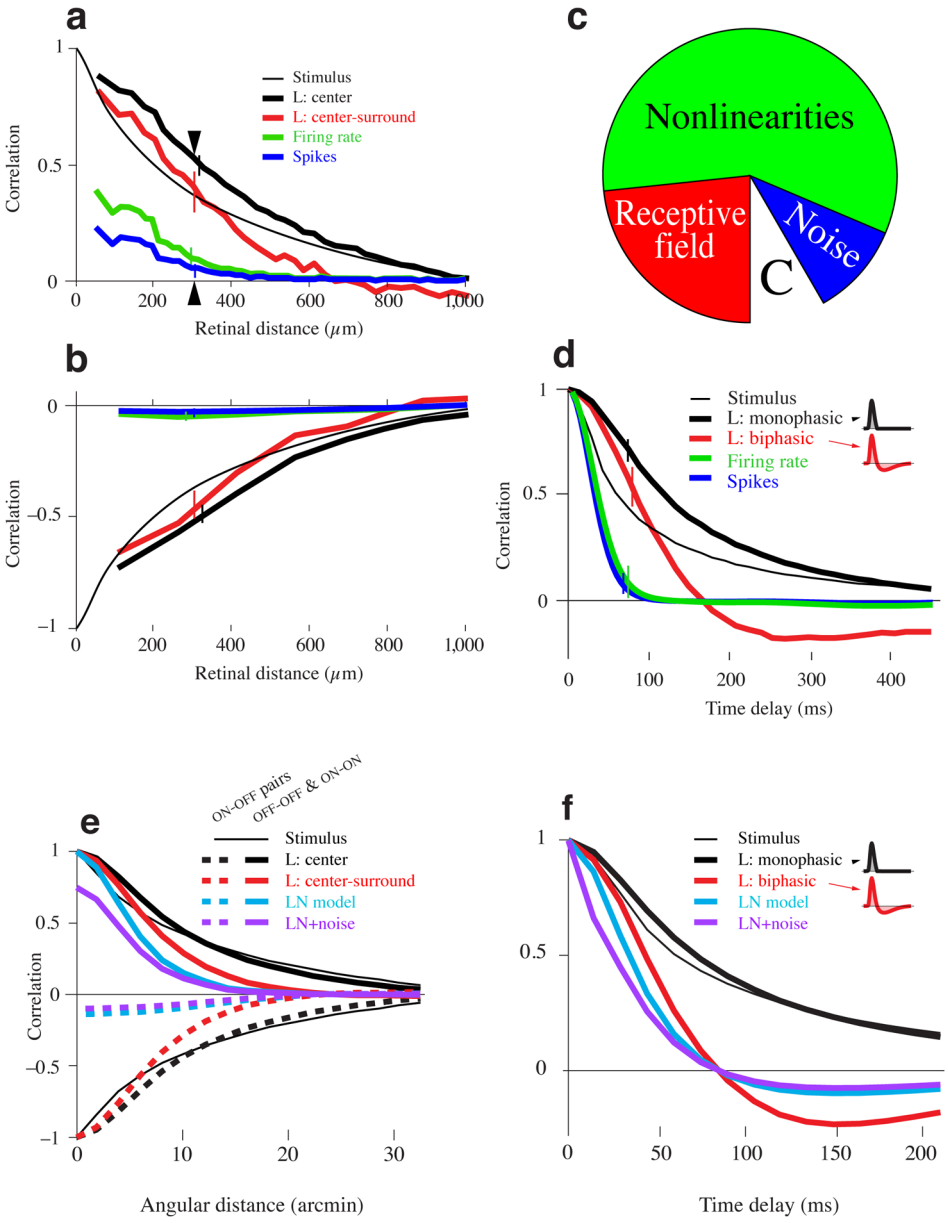

Figure 2.

Nonlinearity accounts for much of decorrelation. **a, b:** Spatial correlation functions for neurons and models under naturalistic stimulation. Cells with the same polarity preference (OFF-OFF or ON-ON pairs) have positive correlations (a) and those with opposite polarity preferences (OFF-ON pairs) have negative correlations (b). Curves are displayed as in Fig. 1h for the stimulus, the trial-averaged firing rates, the spike trains, and linear models. In panel b the stimulus correlations are shown with opposite sign for ease of comparison. Results from many cell pairs are summarized by the median correlation for pairs at similar retinal distance; error bars indicate the central quartiles. **c:** The origins of decorrelation in different response components. The full circle represents the median correlation present in the stimulus after filtering by the receptive field centers, at a retinal distance of 300 μm (arrowheads in panel a). The empty wedge (C) is the much smaller remaining correlation between the ganglion cell spike trains. The red wedge represents the decorrelation caused by

lateral inhibition from receptive field surrounds. The difference between the linear response and the observed firing rate is due to nonlinear processing, and is responsible for over half the decorrelation implemented by the retina (green wedge). The trial-to-trial variation contributes an additional small amount of decorrelation (blue wedge). **d:** Decorrelation in the time domain. Autocorrelation functions of salamander ganglion cell responses and linear models are plotted as a function of delay during naturalistic stimulation. The linear filter's first lobe of ~100 ms width (inset, black) introduced excess correlation beyond that in the stimulus. The antagonistic second lobe (inset, red) counteracted those but overcompensated, introducing anticorrelations at long delays. The observed correlations in the firing rate are much smaller still. **e, f:** Spatial (e) and temporal (f) correlations in macaque retinal ganglion cells, displayed as in (a, b, d). Macaque RGC responses were approximated by an LN model [13,23], using published spatio-temporal receptive field parameters [36] (Eqns 4–6) and sigmoidal nonlinearities [23] (Eqn 10). The output noise was modeled as sub-Poisson variation (Eqn 11) with parameters derived from published spike trains [21] as described in Methods. The stimulus was scaled in space and time to compensate for the different scales of primate and salamander receptive fields. L: Receptive field filter only. LN: including the nonlinearity. LN+noise: including the noise.

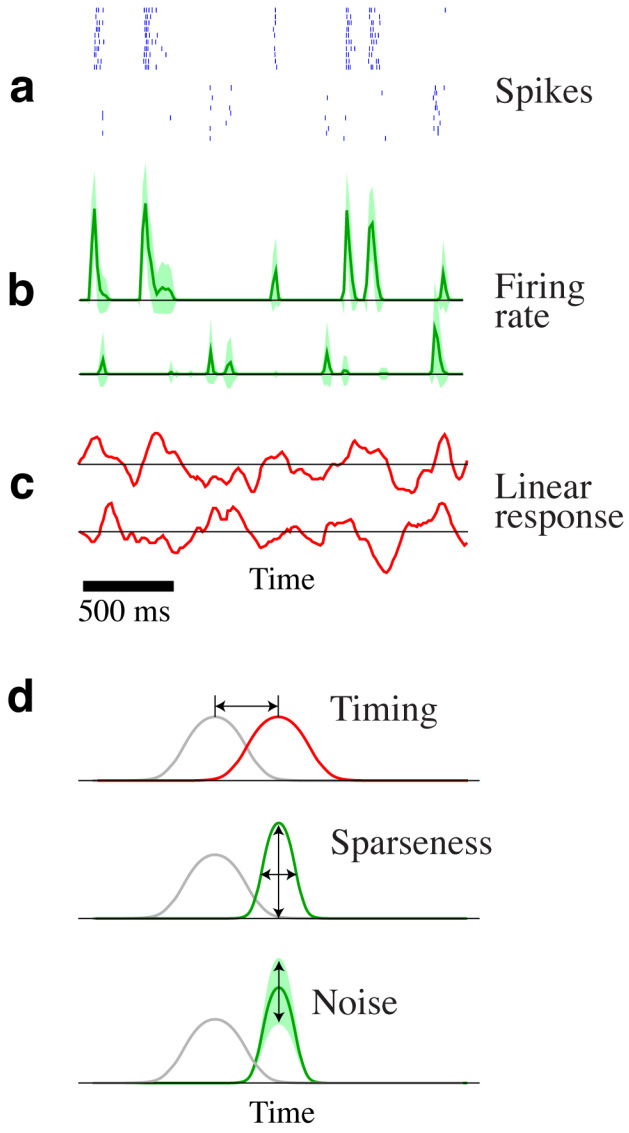

Figure 3.

Sparseness in retinal responses. **a:** Spike rasters for two salamander ganglion cells over 10 repetitions of a naturalistic stimulus. Firing events are brief, separated by long silences, and have some trial-to-trial variability. **b:** Mean firing rates for the same neurons, with shading that indicates the standard deviation about the mean in time bins of 50 ms. **c:** The linear response generated from convolving the stimulus with the spatiotemporal receptive fields of those two cells. This linear model generally captures the times of firing events but differs dramatically in sparseness. **d:** Depiction of three factors contributing to decorrelation between two caricatured neural responses: event timing, sparseness, and noise.

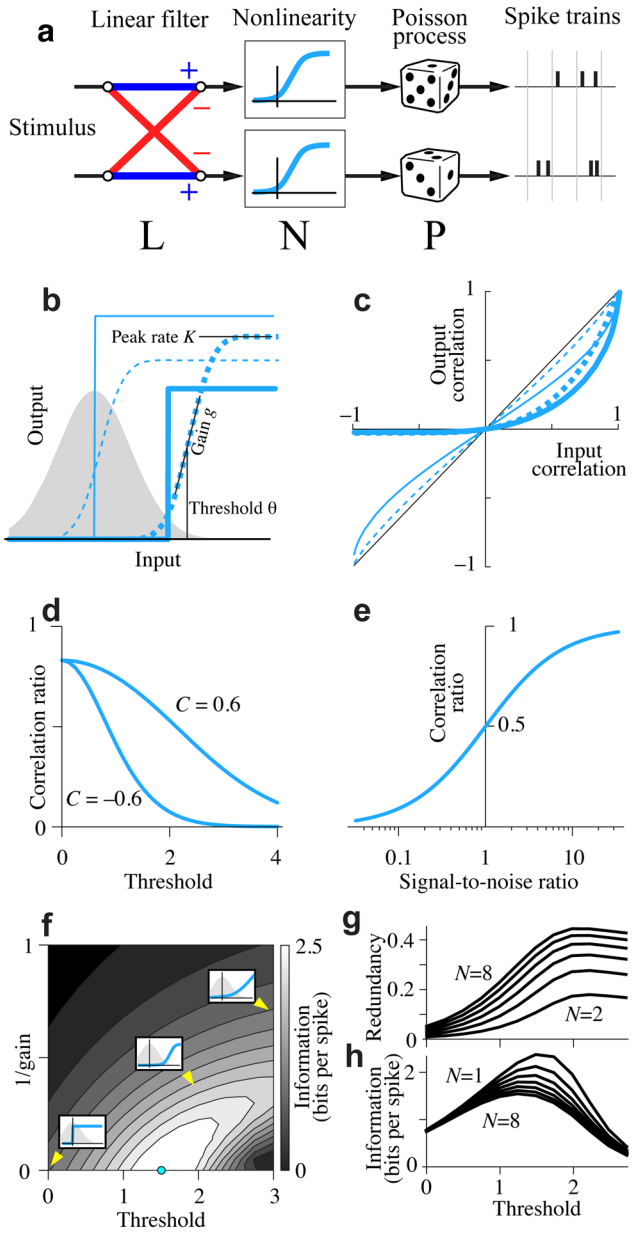

Figure 4.

Decorrelation and efficient coding in the LNP model. **a:** Schematic of two visual neurons that each respond according to the linear-nonlinear-Poisson (LNP) model. For each cell (top and bottom), the stimulus is processed by a linear filter that includes lateral inhibition in space; this signal is passed through a sigmoid nonlinearity; the result modulates the rate of a Poisson process that generates spikes; the spike counts in discrete time windows are the response variable. **b:** Four sample nonlinearities with sigmoid shape and high or low gain (solid or dashed lines), high or low threshold (thick or thin lines), and various peak rates. The shaded curve indicates the probability distribution of the filtered stimulus signal at the input to the nonlinearity. **c:** The effects of such a nonlinear transform on the correlations between two jointly Gaussian variables (see text). Note that the output correlation is always less than that of the input. A low threshold (thin lines) affects the correlation only weakly,

but at high threshold (thick lines) the output correlation is greatly reduced, especially for negative values. The precise shape of the nonlinearity (dashed vs solid) is less important, and the peak rate has no effect. **d:** The ratio of output correlation to input correlation decreases with increasing threshold, shown here for the sigmoid nonlinearity applied to two variables with input correlation $C=\pm 0.6$. **e:** When the two outputs are affected by independent additive noise, this reduces the output correlation by a factor determined by the signal-to-noise ratio (Eqn 14). **f:** Influence of the nonlinearity on information transmission. Within the framework of the LNP model, the threshold and gain of the sigmoid nonlinearity determine how much information about the stimulus is transmitted by the spikes (grayscale and contour lines). The average firing rate was fixed at 1.1 Hz (the median over the salamander ganglion cells). Threshold and 1/gain are measured in standard deviations of the input signal distribution. Insets illustrate nonlinearities (solid lines) at different thresholds and gains relative to the input distribution (shaded area). **g, h:** When multiple neurons receive correlated inputs, raising the threshold makes their outputs more redundant (g) even as the total information increases (h) and correlation decreases (d). All neurons had pairwise correlation coefficients of 0.9, equal thresholds, optimal (infinite) gain, and a fixed mean firing rate of 1.1 Hz. The optimal threshold varies only weakly with population size ($N=1, \ldots,8$).

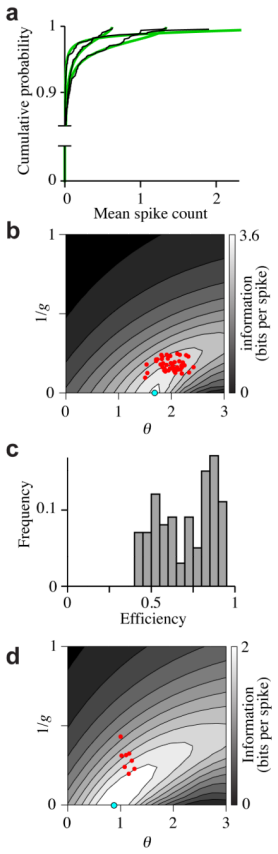

Figure 5.

Efficiency of stimulus coding by retinal ganglion cells. **a:** Cumulative distribution of the spike count in 50-ms time bins, averaged over multiple repeats of the stimulus. Data (thin lines) for three sample ganglion cells and their fit with a model (thick lines) parametrized by θ, g, and K (Eqn 20). **b:** The information transmitted by model firing rate distributions with a fixed mean firing rate of 1.1 Hz, whose shape is parametrized by θ and g. Noise was assumed to be sub-Poisson as observed empirically (Fig. S3, Eqn 11). The blue dot indicates the globally maximal rate of information transmission at this mean rate. Red dots indicate the parameters of the rate distribution measured from salamander ganglion cells. These cells have widely varying mean firing rates. The contour plot of information transmission varies slightly with mean rate, but is shown here for illustration purposes only at one typical mean rate. **c:** Histogram of information efficiencies over the population of salamander retinal ganglion cells. For each cell, the information rate is calculated directly from the empirical spike counts. To calculate efficiency, this information rate is compared to the maximal information rate possible for the measured mean firing rate (Methods). **d:** Information transmission estimated for macaque retinal ganglion cells, displayed as in (b). Red dots are parameters describing the firing rate distribution obtained from published spike rasters in response to white noise stimulation [21]. The contour plot shows the information transmission for different firing rate distributions while fixing the mean rate and time window to typical values, namely 30 Hz and 10 ms respectively.